Optics and Laser Technology 102 (2018) 153–159

Contents lists available at ScienceDirect

Optics and Laser Technology

journal homepage: www.elsevier.com/locate/optlastec

Full length article

Performance analysis of MIMO wireless optical communication system with Q-ary PPM over correlated log-normal fading channel

Huiqin Wang, Xue Wang, Kibe Lynette, Minghua Cao *

School of Computer & Communication, Lanzhou University of Technology, Lanzhou 730050, China

ARTICLE INFO

Article history:
Received 12 January 2017
Received in revised form 8 November 2017
Accepted 22 December 2017
Available online 28 December 2017

Keywords:
MIMO WOC
Spatial correlation
Log-normal fading channel
Ergodic capacity

ABSTRACT

The performance of multiple-input multiple-output wireless optical communication systems that adopt Q-ary pulse position modulation over spatial correlated log-normal fading channel is analyzed in terms of its un-coded bit error rate and ergodic channel capacity. The analysis is based on the Wilkinson's method which approximates the distribution of a sum of correlated log-normal random variables to a log-normal random variable. The analytical and simulation results corroborate the increment of correlation coefficients among sub-channels lead to system performance degradation. Moreover, the receiver diversity has better performance in resistance of spatial correlation caused channel fading.

1. Introduction

Wireless optical communication (WOC) has become an alternative to traditional wireless communication by offering higher transmission rate, inherent security, unlicensed spectrum and lower power consumption [1]. Moreover, multiple-input multiple-output (MIMO) technology is adopted in WOC to further improve the transmission capacity and signal quality [2–6]. Although the linear growth of capacity with the number of antenna indicates the potential of MIMO systems, the true benefits of using multiple antennas may be limited by spatial fading correlation. In practical wireless communication channels, the spatial correlation of multipath fading can no longer be neglected among the antenna elements due to a small aperture size and a long propagation distance as well [7–10]. Therefore, an analysis of MIMO WOC characteristics taking those correlations into account is needed.

Detailed studies of correlation impact on WOC over Gamma-Gamma (G-G) fading channel were proposed in [11–14]. As a matter of fact, a set of criteria for setting the correlation coefficients on small and large scale turbulence components was given in [11]. Further, in [12,13], the authors investigated the effect of fading correlation on bit error rate (BER) and symbol error rate (SER) performance of MIMO WOC systems based on $\alpha-\mu$ approximation method. The outage performance of free space optical (FSO) system using switch-and-stay combining (SSC) diversity over spatially correlated G-G turbulence channels were studied in [14]. It illustrated that the correlation of received signals at different SSC branches could degrade the outage performance by about 1.2 dB. In [15], Navidpour et al. investigated the BER of a MIMO WOC system adopting on-off keying (OOK) modulation over log-normal turbulent fading channels taking the spatial correlation into account. In [16], Hassan Moradi et al. compared different alternatives of switching diversity with N branches and their utilization in performance enhancement over correlated log-normal WOC channels. Subsequently, Hassan Moradi and his colleagues presented the BER performance of correlated dual-branch SSC and switch-and-examine combining scheme under the log-normal WOC channels in [17].

This paper focuses on the BER performance and the ergodic capacity of MIMO WOC communication links over log-normal fading channel when taking the spatial fading correlation into account and using Q-ary pulse position modulation (QPPM). Unlike conventional OOK modulation format, QPPM achieves higher power efficiency and better system performance [18–20].

2. Theoretical analysis

2.1. MIMO WOC system

The block scheme of a MIMO WOC system employing QPPM is shown in Fig. 1. The transmitter consists of M laser diodes (LDs) and a collimator or a telescope to determine the light direction and beam divergence angle. The receiver consists of N lenses and photodetectors (PDs). The lenses focus the received optical field

* Corresponding author.
E-mail address: caomh315@163.com (M. Cao).

https://doi.org/10.1016/j.optlastec.2017.12.038
0030-3992/

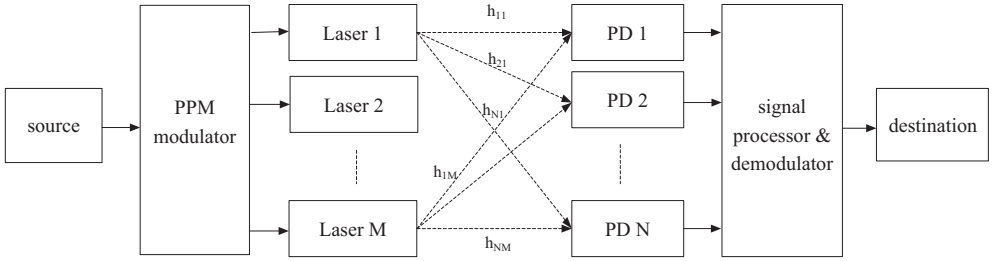

Fig. 1. Block scheme of the MIMO WOC system.

onto a PD. The PD converts the received optical field to an electronic signal for further demodulation.

Assuming the total transmitting power of $M \times N$ (M is the number of LDs, N is the number of PDs) MIMO WOC transmission link is E_s, then the average power of each LD will be E_s/M. During a QPPM symbol period, the symbol interval T_s will be subdivided into Q time slots, each of length $T = T_s/Q$. A digital message comprised of $\log_2 Q$ bits is sent by pulsing the laser in one of these slots.

Assuming the detectors follow Poisson model, which means the signal is transmitting over a flat and slow fading channel. The signal received by the n^{th} detector, denoted as $y^{(n)}$, can be described as

$$y^{(n)} = \frac{n_s}{M}\sum_{m=1}^{M} x^{(m)} h_{nm} + n_b n_0 \tag{1}$$

where $x^{(m)}$, $y^{(n)}$ and n_0 are all $1 \times Q$ vectors, $x^{(m)}$ denotes the signal sent by the m^{th} LD, n_0 denotes the noise vector. n_b denotes the average count rate generated by background noise (include the dark current) and can be described as $n_b = \frac{\eta P_b T}{hf}$, where P_b denotes the average noise power on each detector. h_{nm} denotes the intensity attenuation coefficient from the m^{th} LD to the n^{th} PD due to scintillation. n_s denotes the average number of photoelectrons counted per pulse per laser at one PD for a nonfading channel and can be described as

$$n_s = \frac{\eta P_r T}{hf} = \frac{\eta E_s}{hf} \tag{2}$$

where η denotes the photoelectric conversion efficiency, h denotes the Planck's constant, f denotes the optical carrier frequency, P_r denotes the average receiving power of each detector.

It should be noted that the received signal $y^{(n)}$ consist of a few "on" and "off" time slots. Therefore, we suppose $\lambda_{on,n}$ and $\lambda_{off,n}$ as the average number of photoelectrons observed during an "on" and an "off" time slot at the n^{th} PD, respectively. As a result, Eq. (1) can be converted to the following expression

$$\begin{cases} \lambda_{on,n} = \frac{n_s}{M}\sum_{n=1}^{M} h_{nm} + n_b \\ \lambda_{off,n} = n_b \end{cases} \tag{3}$$

2.2. Log-normal turbulence channel

In a log-normal turbulence channel, the channel fading coefficient can be described as

$$h = \frac{I}{I_0} = \exp(2\chi) \tag{4}$$

where I_0 is the signal light intensity without turbulence, I is the signal light intensity with turbulence. The log-amplitude χ is the normal random variable (RVs) with mean μ_χ and variance σ_χ^2. Therefore, the light intensity fading induced by atmospheric inhomogeneity (turbulence) can be characterized by log-normal distribution [21]. Its probability density function (pdf) will be

$$f_I(h) = \frac{1}{\sqrt{2\pi\sigma_\chi^2}}\frac{1}{2h}\exp\left\{-\frac{\left[\ln(h) - 2\mu_\chi\right]^2}{8\sigma_\chi^2}\right\} \quad h \geq 0 \tag{5}$$

Normalizing the signal light intensity, i.e., $E[I] = 1$, it will satisfy the equation $\mu_\chi = -\sigma_\chi^2$. Furthermore, the scintillation index ($S.I.$) is usually defined to specify the atmospheric channel fading for convenience. It can be defined as Eq. (6) for log-normal fading channel [22]

$$S.I. = \frac{\sigma_I^2}{I_0^2} = \exp(4\sigma_\chi^2) - 1 \tag{6}$$

Its typical value range is [0.4–1.0].

2.3. Correlated log-normal fading channel

The log-amplitude matrix (G) of correlated fading channel can be described as

$$G = R_r S R_t = (g_{nm})_{NM} \tag{7}$$

where $g_{nm} = \ln h_{nm}$, $S = (s_{nm})_{NM}$ is the independent fading channel matrix. s_{nm} denotes the log-amplitude from the m^{th} LD to the n^{th} PD, which is a normal random variable with mean $-0.5\ln(1 + S.I.)$ and variance $\ln(1 + S.I.)$. R_t is the $M \times M$ transmitter correlation matrix, R_r is the $N \times N$ receiver correlation matrix. R_t and R_r can be written as

$$R_r = E\left\{GG^H\right\} = \sum_{c=1}^{M} E\left\{g_c g_c^H\right\} \tag{8}$$

and

$$R_t = E\left\{(G^H G)^T\right\} = \sum_{r=1}^{N} E\left\{g_r^H g_r\right\}^T \tag{9}$$

where g_c and g_r denote the column and row log-amplitude gain of G, respectively.

As a result, we can discuss the spatial correlation channel in three different scenarios:

- Case 1: The independent channel, which means r_t and r_r satisfy $r_t = 0$, $r_r = 0$.
- Case 2: The partial correlated channel, which can be divided into two conditions.
  (1) Only takes the transmitter correlation into account, then $r_t \neq 0$, $r_r = 0$.
  (2) Only takes the receiver correlation into account, then there will be $r_t = 0$, $r_r \neq 0$.
- Case 3: The complete correlated channel, which means both the transmitter and the receiver are correlative. As a result, there are $r_t \neq 0$, $r_r \neq 0$.

In order to make a simple description of spatial correlation, the exponential correlation model can be used to define R_t and R_r [22]

$$R_t = \{r_{ij}\}_{i,j=1,\cdots,M} = \left\{r_t^{|i-j|}\right\}_{i,j=1,\cdots,M} \tag{10}$$

$$R_r = \{r_{ij}\}_{i,j=1,\cdots,N} = \left\{r_r^{|i-j|}\right\}_{i,j=1,\cdots,N} \tag{11}$$

where $|r_t| < 1, |r_r| < 1$ are correlation coefficient of transmitter and receiver, respectively. According to the symmetry of R_t, R_r and the characteristic of the normal distribution, is also a normal random variable with mean $-0.5\ln(1+S.I.)\cdot\left(\frac{1-r_t^M}{1-r_t}\right)\cdot\left(\frac{1-r_r^N}{1-r_r}\right)$ and variance $\ln(1+S.I.)\cdot\left(\frac{1-r_t^{2M}}{1-r_t^2}\right)\cdot\left(\frac{1-r_r^{2M}}{1-r_r^2}\right)$. As a result, the fading channel coefficient follows log-normal distribution. It is obvious that the light intensity fluctuation in a correlated channel can be influenced by the parameters of, $S.I., r_r, r_t, M$ and N.

2.4. Maximum likelihood (ML) detection

Let z_{nq} denotes the observed photoelectrons within time slot q at detector n. Therefore, $Z = \{z_{nq}, n = 1,2,\cdots,N, q = 1,2,\cdots,Q\}$ can be used to represent the set of received observations. If one of Q binary patterns of X_i was launched, the ML decision can then be expressed as

$$\begin{aligned}\hat{X}_i &= \arg\max_{X_i} f(Z|X_i)\\ &= \arg\max_{X_i}\prod_n\left[\frac{\exp(-\lambda_{on,n})(\lambda_{on,n})^{z_{nq}}}{z_{nq}!}\prod_{q\in Q_{off}^{(i)}}\frac{\exp(-\lambda_{off})(\lambda_{off})^{z_{nq}}}{z_{nq}!}\right]\end{aligned} \tag{12}$$

Since the $z_{nq}!$, $\exp(-\lambda_{on,n})$ and $\exp(-\lambda_{off})$ in the expression are invariant to, then they can be removed. The impact to the ML decision outcome can be neglected. As a result, Eq. (12) can be simplified as

$$\hat{X}_i = \arg\max_{X_i}\prod_n\left[(\lambda_{on,n})^{z_{nq}}\prod_{q\in Q_{off}^{i}}(\lambda_{off})^{z_{nq}}\right] \tag{13}$$

The logarithm of Eq. (13) is

$$\begin{aligned}\hat{X}_i &= \arg\max_{X_i}\sum_n\left[z_{nq}\ln(\lambda_{on,n}) + \sum_{q\in Q_{off}^{(i)}} z_{nq}\ln(\lambda_{off})\right]\\ &= \arg\max_{X_i}\sum_n\left[z_{nq}\ln(\lambda_{on,n}) + \sum_{all\ q} z_{nq}\ln(\lambda_{off}) - z_{nq}\ln(\lambda_{off})\right]\\ &= \arg\max_{X_i}\sum_n\left[z_{nq}\ln(\frac{\lambda_{on,n}}{\lambda_{off}})\right]\end{aligned} \tag{14}$$

Substituting Eq. (3) into Eq. (14) results in

$$\hat{X}_i = \arg\max_{X_i}\sum_{n=1}^{N} z_{nq}\ln\left(\frac{\frac{n_s}{M}\sum_{m=1}^{M}h_{nm} + n_b}{n_b}\right) \tag{15}$$

Consequently, the ML detector would make a decision based on a weighted sum over all detectors. On the other hand, the equal gain combining (EGC) can eliminate the need for the channel state information (CSI) at the receiver side of an un-coded MIMO WOC system employing QPPM [3]. For the convenience of subsequent analysis, we form column sums as

$$z_q = \sum_{n=1}^{N} z_{nq}, \quad q = 1,2,\cdots,Q \tag{16}$$

and choose in favor of the largest.

3. Error probability analysis

3.1. Upper bound of BER

Without loss of generality, we assume each laser sends data in the 1st time slot. Error may occurs when the observed photoelectrons z_q in the qth time slot exceeds z_1 in the 1st time slot. The correct decision probability of correlated log-normal fading channel with background radiation is the probability that all z_q(q $\in Q$ and $q \neq 1$) are smaller than z_1, which can be written as

$$P_{correct\ |A} = P[all\, z_q < z_1] = (P[z_2 < z_1])^{Q-1} \tag{17}$$

Consequently, the upper bound of conditional error probability will be

$$\begin{aligned}P_{s|A} &\le 1 - P[all\, z_q < z_1 | slot\ \ 1, A]\\ &= 1 - P[z_2 < z_1 | slot\ \ 1, A]^{Q-1}\\ &= 1 - \left[\sum_{i=1}^{\infty}\sum_{j=0}^{i-1} P(z_1 = i, z_2 = j | slot\ \ 1,\ A)\right]^{Q-1}\end{aligned} \tag{18}$$

where z_1 and z_q indicate the data in "on" and "off" time slots, respectively. Thus, Eq. (18) can be written as

$$P_{s|A} \le 1 - \left[\sum_{i=1}^{\infty}\sum_{j=0}^{i-1}\frac{\left[\left(\frac{n_s}{M}\sum_{m=1}^{M}\sum_{N=1}^{N}h_{nm}\right) + Nn_b\right]^i e^{-\left(\frac{n_s}{M}\sum_{m=1}^{M}\sum_{n=1}^{N}h_{nm}\right)+Nn_b}}{i!} \times\frac{[Nn_b]^j e^{-Nn_b}}{j!}\right]^{Q-1} \tag{19}$$

Note that the upper bound depends on the sum of log-normal RVs $\sum_{m=1}^{M}\sum_{n=1}^{N}h_{nm}$. Abu-Dayya et al. have investigated several approaches that can be utilized to approximate the distribution of a sum of correlated log-normal RVs to a log-normal RV. The investigation demonstrated that Wilkinson's method is the best [23]. Therefore, Wilkinson's method is utilized to simplify the Eq. (19).

Assume

$$H = \begin{pmatrix} e^{g_1} & e^{g_2} & \cdots & e^{g_M}\\ e^{g_{M+1}} & e^{g_{M+2}} & \cdots & e^{g_{2M}}\\ \vdots & \vdots & \ddots & \vdots\\ e^{g_{(N-1)M+1}} & e^{g_{(N-1)M+2}} & \cdots & e^{g_{NM}}\end{pmatrix} \tag{20}$$

and

$$L = e^{g_1} + e^{g_2} + \cdots + e^{g_{NM}} \cong e^{Z} \tag{21}$$

where H is the channel fading matrix, L is a log-normal RV, Z is a normal RV with mean m_z and standard deviation σ_z.

The first-order moment of L can be written as

$$\begin{aligned}u_1 = E[L] = E(e^Z) = E[e^{g_1} + e^{g_2} + \cdots + e^{g_{N\times M}}] = e^{m_z+\sigma_z^2/2}\\ = \sum_{i=1}^{NM} e^{m_{g_i}+\sigma_{g_i}^2/2}\end{aligned} \tag{22}$$

The second-order moment of L can be written as

$$u_2 = E[L^2] = E[e^{2Z}] = E[(e^{g_1} + e^{g_2} + \cdots + e^{g_{N\times M}})^2] = e^{2m_z+2\sigma_z^2}$$
$$= \sum_{i=1}^{NM} E[(e^{g_i})^2] + 2\sum_{i=1}^{NM-1}\sum_{j=i+1}^{NM} E[e^{g_i+g_j}]$$
$$= \sum_{i=1}^{NM} e^{2m_{g_i}+2\sigma_{g_i}^2} + 2\sum_{i=1}^{NM-1}\sum_{j=i+1}^{NM}\{e^{m_{g_i}+m_{g_j}} \cdot e^{\frac{1}{2}(\sigma_{g_i}^2+\sigma_{g_j}^2+2\rho_{ij}\sigma_{g_i}\sigma_{g_j})}\} \quad (23)$$

where ρ_{ij} is the correlation coefficient of g_i and g_j.

It can be derived from Eqs. (22) and (23) that

$$m_z = 2\ln u_1 - \frac{1}{2}\ln u_2 \quad (24)$$

and

$$\sigma_z^2 = \ln u_2 - 2\ln u_1 \quad (25)$$

Therefore, the pdf of L can be written as

$$f(L) = \frac{1}{(2\pi\sigma_z^2)L}\exp\left(-\frac{\ln L - m_z}{2\sigma_z^2}\right) \quad (26)$$

As a result, the Eq. (19) can be simplified as [24]

$$P_{s|L} \le 1 - \left[\sum_{i=1}^{\infty}\sum_{j=0}^{i-1}\frac{[(\frac{n_s}{M}L) + Nn_b]^i e^{-(\frac{n_s}{M}L)+Nn_b}}{i!} \times \frac{[Nn_b]^j e^{-Nn_b}}{j!}\right]^{Q-1} \quad (27)$$

Consequently, the upper bound of expected error probability can be described as

$$P_s = \int P_{s|L} f(L)dL$$
$$\le 1 - \int_0^{\infty}\left[\sum_{i=0}^{\infty}\sum_{j=0}^{i-1}\frac{[\frac{n_sL}{M} + Nn_b]^i e^{-\frac{n_sL}{M}+Nn_b}}{i!} \times \frac{[Nn_b]^j e^{-Nn_b}}{j!}\right]^{Q-1} \cdot f(L)dL \quad (28)$$

Considering that $P_b = ((Q/2)/(Q-1))P_s$ [3], the upper bound of BER can then be expressed as

$$P_b \le \frac{Q}{2(Q-1)} - \frac{Q}{2(Q-1)} \cdot \int_0^{\infty}\left[\sum_{i=1}^{\infty}\sum_{j=0}^{i-1}\frac{[\frac{n_sL}{M} + Nn_b]^i e^{-\frac{n_sL}{M}+Nn_b}}{i!} \times \frac{[Nn_b]^j e^{-Nn_b}}{j!}\right]^{Q-1} \cdot f(L)dL \quad (29)$$

This equation reveals the upper bound of BER related to the parameters of Q, M, N, E_s, E_b, R_t and R_r.

3.2. Numerical investigation

Numerical simulations were carried out by MATLAB with parameters $\eta = 0.5$, $S.I. = 0.6$, $Q = 4$, $\lambda = 1550$ nm and $E_b = -170$ dBJ.

Fig. 2 shows the BER performance of MIMO WOC system in different correlation scenarios. The spatial correlation coefficient is set as 0.6, the number of transmitting antennas and receiving antennas are all set as 2. It is evident from the figure that spatial correlation has a significant impact on the system performance. The influence of transmitter correlation and receiver correlation to system BER are almost the same. The impact of complete correlation is more serious than partial correlation. For example, the complete correlation only has $BER = 10^{-2}$ while the transmitter correlation and receiver correlation have $BER = 10^{-4}$.

Fig. 3 illustrates the BER curves versus E_s with different number of antennas. It can be found from the figure that the receiver diversity has better performance in resistance of antenna correlation caused channel fading. Moreover, it can be discovered from the figure that 1×2 and 2×1 systems have better performance than 1×3 and 3×1 systems over spatial correlated channel. This means that the benefits arising from increasing the number of antennas are not enough to compensate for the loss caused by channel correlation.

Fig. 4 shows the BER curves versus E_s under different correlation coefficients in a 2×2 WOC system. Note that the higher the correlation coefficient the worse the system performance. This indicate that the high channel correlation will seriously affect the system performance.

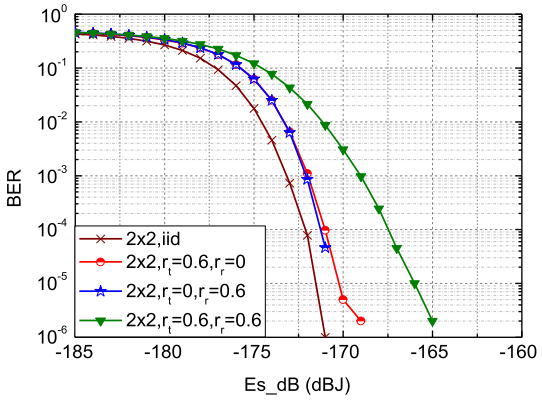

Fig. 2. BER performance of different correlation scenarios.

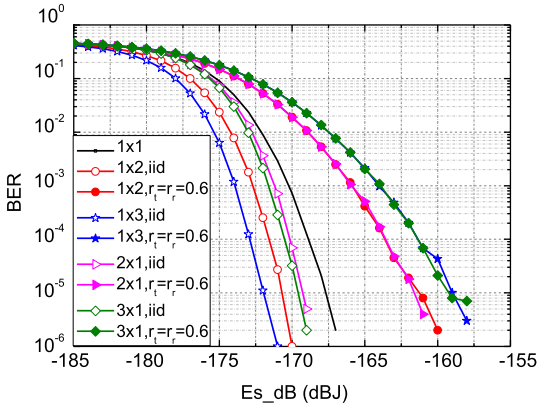

Fig. 3. BER as a function of different number of antennas.

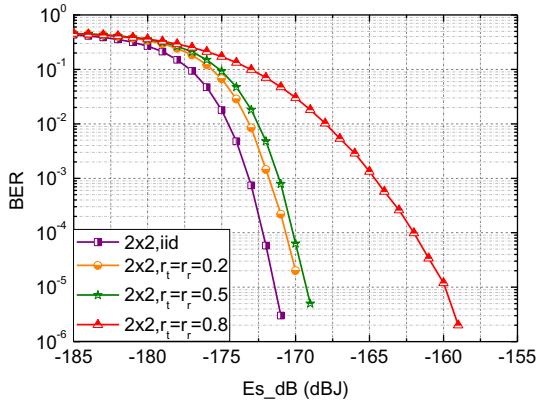

Fig. 4. BER performance of different correlation coefficient over complete correlated channel.

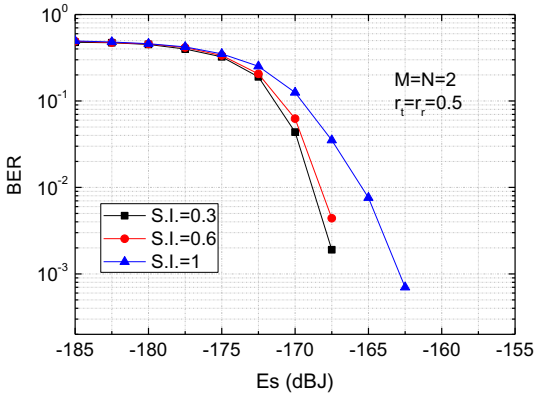

Fig. 5. BER performance for different *S.I.* over complete correlated channel.

Fig. 5 represents the BER of complete correlated MIMO WOC channel with different *S.I.* The increase of *S.I.* leads to worse BER. This indicates that the stronger atmosphere turbulence will seriously affect the correlation channel error performance.

4. Channel capacity

According to Eq. (1), the channel capacity of the optical MIMO system can be defined by

$$C = \max_{p(x)} I(x;y) \tag{30}$$

where $p(x)$ is the pdf of vector x. The mutual information $I(x;y)$ can be described as

$$I(x;y) = H(y) - H(y|x) \tag{31}$$

where $H(y)$ is the entropy of vector y. $H(y|x)$ is the conditional entropy. Mutual information reaches the maximum when the input symbols are equiprobable in a symmetric channel. Consequently, $H(y)$ and $H(y|x)$ can be written as

$$H(y) = \log_2 Q \tag{32}$$

and

$$H(y|x) = \log_2 Q \cdot \exp\left(-\frac{\eta E_s \sum_{m=1}^{M}\sum_{n=1}^{N} h_{nm}}{hfM}\right) \tag{33}$$

Therefore, the instantaneous channel capacity of optical MIMO system without background radiation can be given by

$$C = \log_2 Q \cdot \left[1 - \exp\left(-\frac{\eta E_s \sum_{m=1}^{M}\sum_{n=1}^{N} h_{nm}}{hfM}\right)\right] \tag{34}$$

Eq. (34) reveals that the instantaneous channel capacity is a random variable on fading channel. Therefore, it is a more meaningful way to get the ergodic channel capacity

$$C_{avg} = E[C] = \underbrace{\int_0^\infty \int_0^\infty \cdots \int_0^\infty}_{MN} f(h_{nm}) \log_2 Q \cdot \left[1 - \exp\left(-\frac{\eta E_s \sum_{m=1}^{M}\sum_{n=1}^{N} h_{nm}}{hfM}\right)\right] \underbrace{dh_{11}\cdots dh_{NM}}_{MN} \tag{35}$$

It is complex to perform the $M \times N$-fold integration. As in Section 3, we approximate the sum of log-normal RVs $\sum_{m=1}^{M}\sum_{n=1}^{N} h_{nm}$ as another log-normal RV L. Thus, the ergodic channel capacity of correlated optical MIMO system can be written as

$$C_{avg} = E_H(C) = \int_0^\infty f(L) \log_2 Q \cdot \left[1 - \exp\left(-\frac{\eta E_s L}{hfM}\right)\right] dL \tag{36}$$

The approximation is much simpler than its former version since it only requires a single integration. As a result, it can be further simplified as

$$C_{avg} = \log_2 Q - \log_2 Q \cdot \int_0^\infty f(L) \exp\left(-\frac{\eta E_s L}{hfM}\right) dL \tag{37}$$

To further illuminate the ergodic channel capacity of MIMO WOC communication systems, comparisons of the foregoing analysis and equations under different correlation mechanisms and correlated coefficients were carried out.

Fig. 6 shows the ergodic channel capacity with different number of time slots when using QPPM. Both exact and approximate expressions (Eqs. (35) and (37)) are depicted in the figure. It is evident from the figure that the curves of approximate ergodic channel capacity are close enough to the corresponding exact curves. Note that the computation complexity of approximate ergodic channel capacity is lower than the exact one. Therefore, the slight performance loss is acceptable for the approximation.

Fig. 7 shows the ergodic channel capacity of a 4×4 MIMO WOC system with different correlation coefficients ranging from 0.1 to 0.9, where the parameters are set as follows, $\eta = 0.5$, $Q = 8, S.I. = 0.6$ and $\lambda = 1550$ nm. The curves of independent

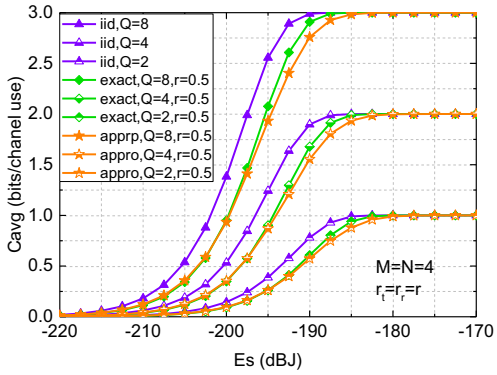

Fig. 6. The impact of channel correlation on the ergodic channel capacity with different number of time slots.

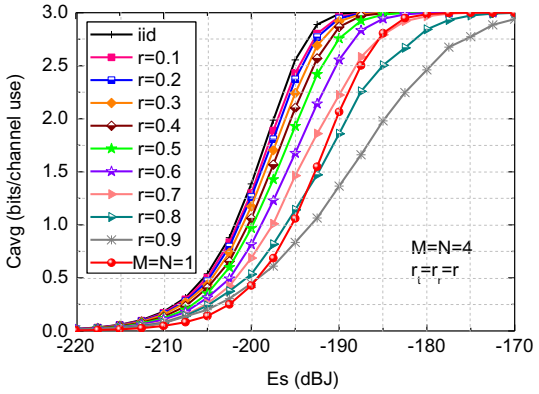

Fig. 7. Ergodic channel capacity for different correlation coefficients.

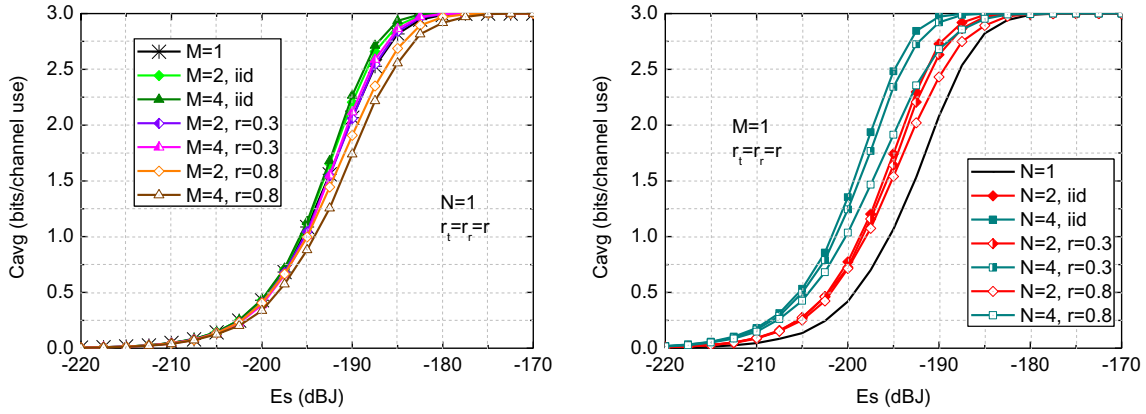

(a) Transmission diversity (b) Reception diversity

Fig. 8. The influence of antenna numbers to ergodic channel capacity over partial correlated channel.

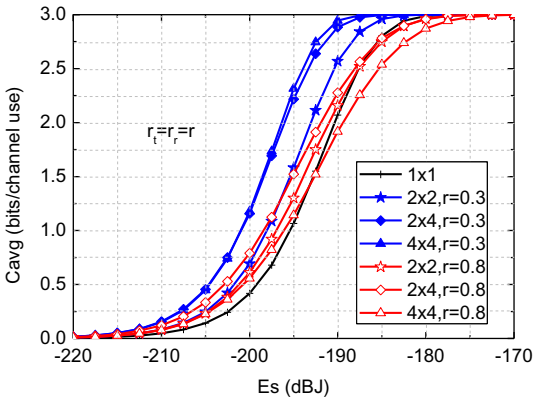

Fig. 9. The ergodic channel capacity of complete correlated MIMO WOC channel.

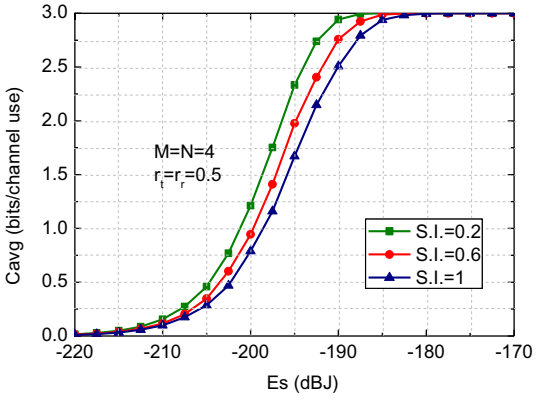

Fig. 10. The ergodic channel capacity of correlated MIMO WOC channel with different *S.I.*

4×4 MIMO WOC system and single input single output (SISO) system are also presented for comparison. As anticipated earlier, the independent system has the best performance. The ergodic channel capacity reduces slightly when the correlation coefficient r is small. The ergodic channel capacity reduction becomes significant when $r > 0.5$. The ergodic channel capacity is even lower than that of SISO system when $r > 0.8$.

Fig. 8 demonstrates the influence of different antenna numbers to the ergodic channel capacity. When there is only one receiving antenna, as shown in Fig. 8(a), the influence increases with the increasing of transmitting antenna numbers. Particularly, in strong correlated channel (i.e. $r = 0.8$), the increase of transmitting antenna number will result in channel capacity reduction. The benefits arising from transmitting antenna number increasing are not enough to compensate for the channel correlation caused loss. Fig. 8(b) shows the influence of different receiving antenna numbers to the channel capacity when there is only one transmitting antenna. Obviously, the ergodic channel capacity increment brought by reception diversity is much higher than the loss caused by spatial channel correlation.

Fig. 9 represents the ergodic channel capacity of complete correlated MIMO WOC channel when $r \in \{0.3, 0.8\}$. Note that in a weak spatial correlated channel, the ergodic channel capacity increases significantly with the antenna number increasing. But in a strong spatial correlated channel, the ergodic channel capacity suffers more damage with more antennas, which is reflected in worse system performance. Furthermore, its performance is even worse than that in SISO systems at high launch power. Therefore, MIMO technology is not an ideal solution for strong spatial correlated channels.

Fig. 10 shows the ergodic channel capacity of correlated MIMO WOC channel with different *S.I.* As one might expect, the strong atmosphere turbulence will reduce the ergodic channel capacity.

5. Conclusion

We analyzed a correlated MIMO WOC system employing QPPM over log-normal fading channel. The analytic expressions for both error bit rate and ergodic channel capacity have been derived with the help of Wilkinson's method. The analysis shows the unfavorable effects from spatial channel correlation of multiple antennas and detectors. Reception diversity is found to be more competent to resist spatial channel correlation compared to transmission diversity. This work may helpful to configure the antennas of MIMO WOC system rationally.

Acknowledgments

This work was in part supported by NSFC Program (61465007 and 61265003), Foundation of Gansu Educational Committee (2017A-011), Specialized Research Fund for the Doctoral Program of Higher Education of LUT (03-061616).

References

[1] X. Zhu, J.M. Kahn, Free-space optical communication through atmospheric turbulence channels, IEEE Trans. Commun. 50 (8) (2002) 1293–1300, https://doi.org/10.1109/TCOMM.2002.800829.

[2] Bayaki Ehsan, Schober Robert, R.K. Mallik, Performance analysis of MIMO free-space optical systems in gamma-gamma fading, IEEE Trans. Commun. 57 (11) (2009) 3124–3224, https://doi.org/10.1109/TCOMM.2009.11.080168.

[3] S.G. Wilson, M. Brandt-Pearce, Q. Cao, Free-space optical MIMO transmission with Q-ary PPM, IEEE Transmission Commun. 53 (8) (2005) 1402–1412, https://doi.org/10.1109/TCOMM.2005.852836.

[4] S.G. Wilson, M. Brandt-Pearce, Q. Cao, Optical repetition MIMO transmission with multi-pulse PPM, IEEE J. Sel. Areas Commun. 23 (9) (2005) 1901–1910, https://doi.org/10.1109/JSAC.2005.853804.

[5] A. Luong Duy, T. Pham Anh, Average capacity of MIMO free-space optical gamma-gamma fading channel, IEEE Int. Conf. Commun. (2014) 3354–3358, https://doi.org/10.1109/ICC.2014.6883839.

[6] Nick Letzepis, Ian Holland, William Cowley, The Gaussian free space optical MIMO channel with Q-ary pulse position modulation, IEEE Trans. Wireless Commun. 7 (5) (2008) 1744–1753, https://doi.org/10.1109/TWC.2008.061002.

[7] Zhixiao Chen, Song Yu, Tianyi Wang, Wu Guohua, Shaoling Wang, Wanyi Gu, Channel correlation in aperture receiver diversity systems for free-space optical communication, J. Opt. 14 (12) (2012) 1–7, https://doi.org/10.1088/2040-8978/14/12/125710.

[8] G.W. Yang, M.A. Khalighi, Z. Ghassemlooy, S. Bourennane, Performance analysis of space-diversity free-space optical systems over the correlated Gamma-Gamma fading channel using Pade approximation method, IET Commun. 8 (13) (2014) 2246–2255, https://doi.org/10.1049/iet-com.2013.0962.

[9] T. Ozbilgin, M. Koca, Inter-aperture correlation in MIMO free space optical systems, Opt. Commun. 353 (2015) 139–146, https://doi.org/10.1016/j.optcom.2015.05.025.

[10] J.A. Anguita, M.A. Neifeld, B.V. Vasic, Spatial correlation and irradiance statistics in a multiple-beam terrestrial free-space optical communication link, Appl. Opt. 46 (26) (2007) 6561–6571, https://doi.org/10.1364/AO.46.006561.

[11] G. Yang, M.A. Khalighi, Z. Ghassemlooy, S. Bourennane, Performance evaluation of receive-diversity free-space optical communications over correlated Gamma-Gamma fading channels, Appl. Opt. 52 (24) (2013) 5903–5911, https://doi.org/10.1364/AO.52.005903.

[12] G. Yang, M.A. Khalighi, S. Bourennane, Z. Ghassemlooy, Fading correlation and analytical performance evaluation of the space-diversity free-space optical communications system, J. Opt. 16 (3) (2014) 035403, https://doi.org/10.1088/2040-8978/16/3/035403.

[13] H.S. Khallaf, J.M. Garrido-Balsells, H.M.H. Shalaby, Seiichi Sampei, SER analysis of MPPM-coded MIMO-FSO system over uncorrelated and correlated gamma-gamma atmospheric turbulence channels, Opt. Commun. 356 (2015) 530–535, https://doi.org/10.1016/j.optcom.2015.08.060.

[14] M. Petkovic, J. Anastasov, G.T. Djordjevic, P. Ivanis, Impact of correlation on outage performance of FSO system with switch-and-stay diversity receiver, in: 2015 IEEE International Conference on Communications (ICC), London, 2015, pp. 2756–2761, doi: 10.1109/ICC.2015.7248743.

[15] S. Mohammad Navidpour, Murat Uysal, Mohsen Kavehrad, BER performance of free-space optical transmission with spatial diversity, IEEE Trans. Wireless Commun. 6 (8) (2007) 2813–2819, https://doi.org/10.1109/TWC.2007.06109.

[16] Hassan Moradi, Hazem H. Refai, Peter G. LoPresti, Switched diversity approach for multi-receiving optical wireless systems, Appl. Opt. 50 (29) (2011) 5606–5614, https://doi.org/10.1364/AO.50.005606.

[17] H. Moradi, H.H. Refai, P.G. Lopresti, Switch-and-stay and switch-and-examine dual diversity for high-speed free-space optics links, IET Optoelectron. 6 (1) (2012) 34–42, https://doi.org/10.1049/iet-opt.2011.0007.

[18] Hsun-Hung Chan et al., Performance of optical wireless OOK and PPM systems under the constraints of ambient noise and multipath dispersion, IEEE Commun. Mag. 36 (12) (1998) 83–87, https://doi.org/10.1109/35.735882.

[19] G.A. Mahdiraji et al., Comparison of selected digital modulation schemes (OOK, PPM and DPIM) for wireless optical communications, in: 2006 4th Student Conference on Research and Development, 2007, pp. 5–10, doi: 10.1109/SCORED.2006.4339297.

[20] N. Wu, X. Wang, H. Dai, Performance of indoor visible light systems using OOK and PPM modulations under multipath channels, 2013, pp. 84–88. doi: 10.1109/IWOW.2013.6777783.

[21] H. Moradi, M. Falahpour, H.H. Refai, P.G. LoPresti, M. Atiquzzaman, BER analysis of optical wireless signals through lognormal fading channels with perfect CSI, IEEE, Int. Conf. Telecommun. (2010) 493–497, https://doi.org/10.1088/1367-2630/12/4/045024.

[22] Z. Ghassemlooy, W. Popoola, S. Rajbhandari, Optical Wireless Communication: System and Channel Modelling with Matlab, CRC Press Inc, 2013, doi:10.1201/b12687-2/r10.1201/b12687-2.

[23] S.L. Loyka, Channel capacity of MIMO architecture using the exponential correlation matrix, IEEE Commun. Lett. 5 (9) (2001) 369–371, https://doi.org/10.1109/4234.951380.

[24] A.A. Abu-Dayya, N.C. Beaulieu, Outage probabilities in the presence of correlated lognormal interferers, IEEE Trans. Veh. Technol. 43 (1) (1994) 164–173, https://doi.org/10.1109/25.282277.